SiP-based SSBI Cancellation for OFDM

Mingyang Lyu, Wei Shi, and Leslie A. Rusch

IEEE Photonics Journal (1 May 2019)

Doi: 10.1109/JPHOT.2019.2911027

https://ieeexplore.ieee.org/document/8703741

SiP-based SSBI Cancellation for OFDM

Mingyang Lyu, *Student Member, IEEE*, Wei Shi, *Member, IEEE*, Leslie Rusch, *Fellow, IEEE*

Centre for Optics, Photonics, and Lasers (COPL), ECE department, Université Laval, Québec, QC, G1V 0A6, Canada
Email: rusch@gel.ulaval.caA

This research was funded by TELUS Corp., Aeponyx, Quebec provincial funding from PROMPT, and grant number CRDPJ 499664 from the Natural Science and Engineering Research Council of Canada.

Abstract: We propose for the first time to use a silicon photonics (SiP) solution for a passive optical network to both reduce signal-signal beat interference (SSBI) and recuperate a part of the downlink carrier for use in the uplink. The Kramers-Kronig (KK) receiver for direct detection of advanced modulation formats overcomes SSBI at the cost of a moderate carrier to signal ratio ($>$6 dB) and high oversampling ($4\times$). We propose an optical SSBI solution that achieves better performance than KK and requires only standard sampling and low (3 dB) carrier to signal power ratio. The receiver is conceived for the downlink in passive optical networks, where carrier signal must be husbanded for re-use in the uplink. Using cost effective and power efficient SiP, the receiver filters the incoming signal, suppresses SSBI, and routes a portion of the carrier for use in the uplink.

We experimentally examine the SSBI suppression in this paper. While previous demonstrations used bulky, discrete components, we achieve significant Q-factor improvement with a simple SiP solution. We examine the optimal frequency offset between the carrier and the microring resonator center frequency. The robustness to frequency drift, as well as the impact of imperfect filtering, is discussed and quantified.

Index Terms: Signal Processing; SSBI; Optical Communication

1. Introduction

Coherent detection has whetted our appetite for higher bandwidth communications, but we also crave the low cost of direct detection. One solution for high bit rate with direct detection is the use of optical orthogonal frequency division multiplexed (OFDM) with a distributed carrier; however, performance is limited by signal to signal beat interference (SSBI). Quadrature amplitude modulation (QAM) or OFDM can also be achieved with direct detection when using the Kramer-Kronig (KK) receiver. We propose a simple, integrated subsystem that can suppress SSBI in OFDM, without the DSP and high oversampling required for KK reception.

Optical OFDM is a promising solution for passive optical networks (PONs), as it is particularly flexible in sculpting both time and frequency resources. To avoid fading that is induced by chromatic dispersion [1], PONs could use single side-band (SSB) OFDM. As PONs require low cost user equipment, direct detection (DD) of optical OFDM is the preferred solution. In direct detection, beating between signal and carrier generates the desired OFDM signal, however, beating among the OFDM subcarriers (signal-to-signal beat interference or SSBI) obscures the desired part of the electrical spectrum. It is the major source of impairment in DD-SSB-OFDM systems.

There are several approaches to deal with SSBI in digital signal processing. Most recently linearization filtering is used, whereby the SSBI is estimated from the received signal and sub-

National Science and Engineering Research Council of Canada (NSERC) Funding: CRDPJ 499664

tracted before data detection [2], [3]. These approaches exploit the deterministic nature of SSBI, and have been applied to discrete multi-tone (a variety of OFDM) [2] and QAM modulation [3]–[5]. An experimental comparison in [6] concluded that the KK DSP method yielded better performance than DSP linearization.

All direct detection solutions, whether OFDM or QAM, optical or digital SSBI suppression, use a carrier stronger than the signal to enhance reception. In KK the carrier to signal power ratio (CSPR) should be above 6 dB for bit error rate (BER) on the order of 10^{-2} with 6-8 samples per symbol. [7]. Upsampling (after reception at the standard two samples per symbol for SSB-OFDM) is required due to the square-root and logarithm operations in KK. There have been many examinations of the effect of CSPR and upsampling rate on BER for KK. The performance falls off precipitously for CSPR below 6 dB, and severe penalties are incurred for moderate upsampling (2.5-3$\times$) [8].

Several solutions have been proposed to enhance KK, including an optical sub-assembly whose complexity is similar to that in this paper [9]. Using this optical sub-assembly for KK, the sampling rate was reduced to the standard two samples per symbol and BER $\sim 10^{-2}$ was achieved at CSPR of 3 dB. However, additional DSP was required, as well as the optical sub-assembly; a gradient descent optimization in DSP involved thousands of iterations.

We propose for the first time to use a SiP solution to both reduce SSBI and recuperate a part of the downlink carrier for use in the uplink. In cost-effective, single-feeder PONs, the carrier is reused for uplink modulation to achieve colorless operation. Methods using high CSPR are not suitable in these PONs. The carrier reuse limits the CSPR power budget. The portion of carrier power reserved for direct detection may not be sufficient to meet the KK carrier amplitude requirements, i.e., minimum phase. This is particularly true for KK receivers for OFDM, whose greater peak to average ratio would require even greater CSPR than that reported when using QAM modulation with KK.

We address the significant challenge in working with low-cost SiP filtering for SSBI cancellation. We focus on the microring resonator (MRR) structure for the SSBI suppression on the through port, as the MRR can also provide downlink carrier recovery on the drop port. In this paper we focus on the through port filtering performance, which must be designed for robustness against temperature induced frequency drift. We examine experimentally an MRR subsystem designed for both SSBI cancellation and carrier reuse.

We first discuss the details of the fabricated integrated SSBI cancellation subsystem in section II. In section III we examine the non-ideal filtering effect that could undermine the cancellation performance. System simulation were completed to predict the performance. In section IV we discuss the design and characterization of the micro ring resonator for carrier suppression. After a description of the experimental setup, performance improvement using SiP SSBI cancellation system is evaluated experimentally. Several optimal choices for the system operating point are identified.

2. System design

Optical SSBI cancellation in OFDM is both 1) appropriate for PONs and 2) high performance. In these approaches, optical signal processing creates a copy of the SSBI. The SSBI signal is isolated optically, photodetected, and its electrical version is subtracted from the photodetected signal corrupted by SSBI; the resulting signal is free of SSBI. This has been examined analytically [10] and experimentally using discrete components [11].

The only experimental optical approaches for SSBI cancellation in the literature have had high system complexity due to the use of discrete components. We examine the use of silicon photonics to overcome this limitation. We propose an integrated SSBI cancellation subsystem in SiP to avoid drawbacks of using discrete components. We demonstrated the first proof-of-concept for silicon photonics (SiP) SSBI cancellation at MWP 2017 [12] using micro ring resonators (MRRs). That demonstration used cascaded MRRs, whose low extinction ratio and wide bandwidth limited the

National Science and Engineering Research Council of Canada (NSERC) Funding: CRDPJ 499664

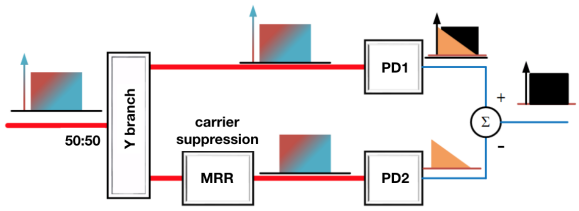

Fig. 1: Optical SSBI cancellation scheme with ideal carrier suppression

SSBI cancellation.

In Fig. 1 we illustrate SSBI cancellation in the the optical domain proposed by [10]. The signal with mixed polarization (frequency domain rectangle with gradient fill) is sent to a power splitter, i.e., y branch. One is directly sent for detection, where we will get the detected signal as well as SSBI. The other path is sent to a filter that suppresses the carrier, but passes the data. Without the carrier, i.e., with ideal carrier suppression, we detect the SSBI alone. By subtracting the SSBI from the through path output, we can realize SSBI cancellation.

The discrete component approach is limited by excessive losses and by unequal delays which are difficult to equalize (keeping the two paths exactly the same length). Therefore, we turn to integrated solutions to avoid those drawbacks. The frequency response of the MRR to suppress the carrier is a notch. Ideally, we suppress the carrier and leave data unchanged [13]. The Y branch is used to split the light into two paths. A polarization controller is required, as generally SiP components are sensitive to polarization, while the light coupled into the chip arrives with an arbitrary polarization state. Integration ensures that 1) all paths are produced with similar lengths, 2) any environmental changes are experienced simultaneously on all components, and 3) cost is low and footprint is small. As the optical path on-chip is only several millimetres, the fabrication mismatch of the two paths will be negligible.

The hardware requirements for optical SSBI cancellation call for an additional photodetector vis-a-vis a conventional receiver with digital SSBI cancellation. However, digital processing alone approaches (including the KK receiver) require at least moderate CSPR. We will show optical signal processing can suppress SSBI even at 0 dB CSPR. To lower the minimal KK CSPR (~ 6 dB), an enhanced KK receiver was proposed in [9]. For enhanced KK, the signal is split into two branches, as in our solution. Dispersive material is used to differentiate the two branches, and then the standard KK procedure is applied to both branches. With an additional gradient descent algorithm in DSP, the performance can be optimized to reduce required CSPR by 3 dB. This reduction is still not as great as the one we demonstrate with optical SSBI suppression. In addition, we avoid the DSP costs (high iterations of the gradient descent algorithm) in the enhanced KK receiver. Our proposed subsystem is a better solution when low CSPR is critical, as in a PON that reuses the carrier for the uplink.

3. The effect of non-ideal filtering effect

In this section we examine the impact of imperfect filtering on the SSBI cancellation efficiency. Two factors enter into consideration: 1) the finite roll-off of the filter, and 2) the frequency offset of the carrier from the notch center frequency. We examine via simulation the impact of the first as a function of κ (the coupler design of the MRR) and the second as a function of the detuning between signal and filter. In later sections we will confirm our simulation results experimentally.

3.1. Spectral effects

An illustration of the electrical spectrum after PD1 (from Fig. 1) is shown in Fig. 2a; it consists of the desired OFDM signal (rectangular) and the SSBI (triangular). Fig. 2b shows the electrical

National Science and Engineering Research Council of Canada (NSERC) Funding: CRDPJ 499664

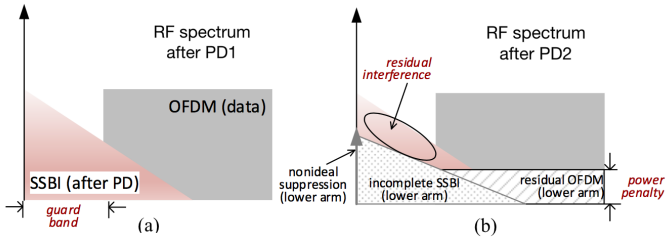

Fig. 2: Non-ideal filtering effect

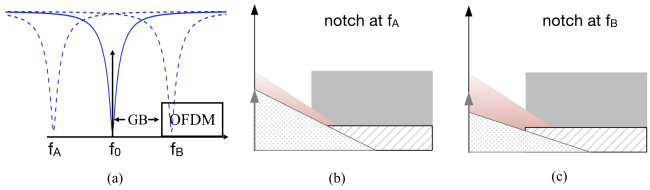

Fig. 3: a) Carrier and OFDM placement vis-à-vis offsets. Electrical spectrum components for different cases of frequency offset, b) notch at carrier, c) notch more distant from OFDM signal, and d) notch closer to OFDM signal

spectrum at PD2 in hashed regions, superimposed on Fig. 2a spectrum. Although the carrier is located exactly on the notch, the effect of a non-ideal frequency response, $H(f)$, is visible: there is a residual carrier and thus residual OFDM. After subtracting the RF spectrum at PD2 from the RF spectrum at PD1, these residuals result in a power penalty. Because the OFDM signal sees non-flat frequency response, the SSBI reconstruction is also incomplete at PD2. This causes incomplete SSBI cancellation.

As the filtering effect can arise from center frequency offset, consider three frequency offset scenarios shown in Fig. 3a: no frequency offset, offset f_A to frequencies far from the OFDM signal, offset f_B to frequencies close to the OFDM signal. When there is no frequency offset, the RF output spectra are shown in Fig. 2b. The carrier sees maximum suppression, and the OFDM band suffers limited filtering effects.

When the notch is at f_A, the RF output spectrum, shown in Fig. 3b has a prominent carrier and the OFDM band is little changed. The presence of the carrier leads to residual OFDM at PD2, hence a greater power penalty. The SSBI reconstruction is improved since the OFDM signal was less distorted by $H(f - f_A)$. These two opposite influences will moderate the overall performance, and may even lead to better performance for this type of offset.

When the notch is at f_B, the RF output spectrum is as illustrated in Fig. 3c. As with case f_A, there is a prominent residual carrier; case f_A and f_B see the same increased power penalty.The OFDM band ,however, sees much stronger filtering than either case f_0 or f_A. This leads to worse SSBI reconstruction, thus the performance will drop fast.

3.2. Simulation setup

We investigate the non-ideal filtering effect with the simulator model illustrated in Fig. 4. We generate 16 Gbaud QPSK single side-band OFDM signal over 256 subcarriers. We do not use a guard band. We add a carrier to achieve 5 dB CSPR. Amplified spontaneous emission (ASE) noise in the form of additive white Gaussian noise is added to adjust the optical signal to noise ratio (OSNR) to 25 dB. To emulate the optical SSBI cancellation procedure, we divide the signal into two parts with equal power. One part is directly detected by a square law PD. The other part is filtered by a MRR to suppress the carrier. The MRR frequency response, $H(f)$, is simulated using the transfer matrix method. Various coupling coefficients κ, the coupling coefficient of the

National Science and Engineering Research Council of Canada (NSERC) Funding: CRDPJ 499664

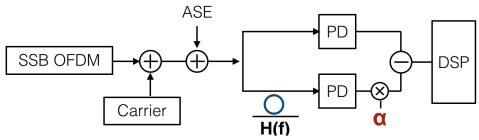

Fig. 4: Simulation system setup

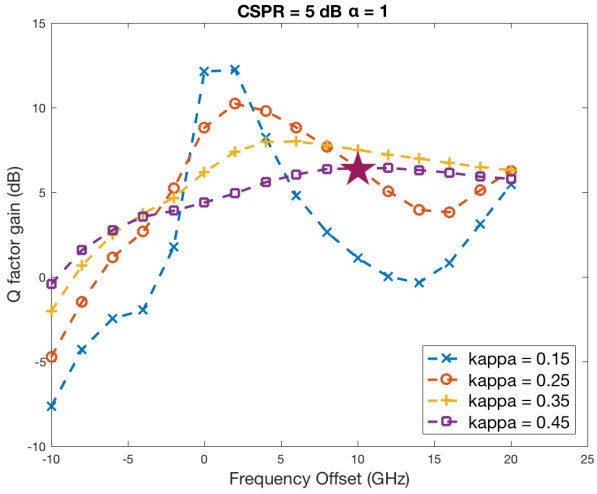

Fig. 5: Simulation of SSBI cancellation performance via different frequency offsets (α = 1)

bus-resonator coupler, are examined. After carrier suppression, the reconstructed SSBI is used to cancel SSBI in the through path.

For each subcarrier we count errors, N_{err}, over the 10^5 symbols transmitted. We also calculate average error vector magnitude (EVM) for the QPSK constellation. To improve accuracy [14], we estimate bit error rate (BER) from both counted errors and the average EVM per

$$BER = \begin{cases} N_{err}/10^5 & \text{for } N_{err} \geq 10 \\ \frac{1}{2}\text{erfc}\left(1/\sqrt{2}EVM\right) & \text{for } N_{err} < 10 \end{cases} \quad (1)$$

where the erfc is the complementary error function. The Q-factor for QPSK is found from the estimated BER per

$$Q = \sqrt{2}\text{erfc}^{-1}(2\text{BER}) \quad (2)$$

The Q-factor gain after SSBI cancellation with different frequency offsets is shown in Fig. 5. Very negative frequency offset sees little improvement, and in fact, sees mostly negative Q-factor gain, i.e., worse performance. This confirms our discussion of the scenario in Fig. 2c. As frequency offset approaches zero, we are more likely to see positive gain, again matching our discussion in the previous section, this time for the scenario in Fig. 2b. For positive frequency offset, the trade-off between non-ideal carrier suppression and undesired filtering on OFDM will give us a sweet spot that is highly dependent on MRR design.

3.3. Scaling factor α

The original SSBI cancellation calls for subtraction of the two photodetector outputs. We introduce a new parameter, scaling factor α, to create a scaled SSBI estimate. Given the competing

National Science and Engineering Research Council of Canada (NSERC) Funding: CRDPJ 499664

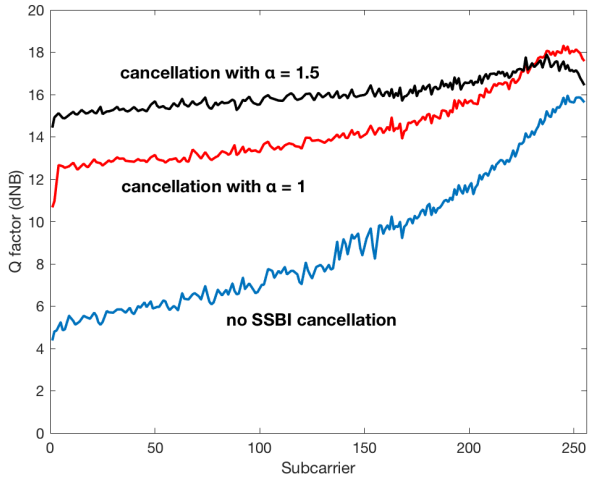

Fig. 6: Simulation of Q-factor per subcarrier with varying α for κ = 0.45 and 10 GHz frequency offset

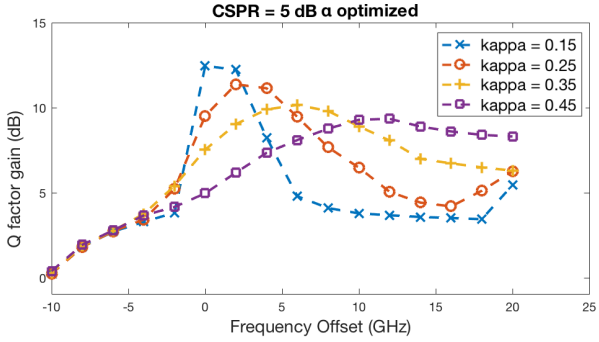

Fig. 7: Simulation of SSBI cancellation performance via different frequency offsets (α optimized)

contributions of imperfect filtering, it is possible that we can improve performance by subtracting a scaled version of the SSBI estimate. For this reason, we examine the use of α in the MRR branch after photodetection. This additional degree of freedom could counterbalance, to some extent, the variation in Q-factor due to frequency offset. We note in passing that the linearization filter method as well as enhanced KK receiver used a parameter similar to α to optimal SSBI estimation.

We sweep the α from 0.1 to 1.5 with a step of 0.1. The point ($\kappa = 0.45$, 12 Ghz offset) marked with a star in Fig. 5 is the one detailed in Fig. 6. The blue curve in Fig. 6, no SSBI cancellation, has lower-index subcarriers suffering stronger SSBI; the Q-factor increases as the subcarrier index increases. For SSBI cancellation with α = 1, red curve, the performance per subcarrier is more uniform. Due to the incomplete SSBI cancellation, the lower-index subcarriers still perform worse than others. The best overall SSBI cancellation is found for α_{opt} =1.5, black curve. The performance is much more uniform across carriers. Gains in lower-index subcarriers translate to overall improvement despite a small dip in performance at the highest index subcarriers.

In Fig. 7 we recreate the Q-factor gain from Fig. 5, but this time using the optimal alpha (a different α for each data point). Comparing Fig. 5 with Fig. 7, we avoid degraded performance. Considering all κ simulated, positive gain can be increased by 1.2 dB on average. In general, the gain improves most for larger κ. For $\kappa = 0.45$, the positive gain increases by 2.01 dB on average,

National Science and Engineering Research Council of Canada (NSERC) Funding: CRDPJ 499664

with a maximum increase of 2.92 dB. While there is some improvement in the maximum Q-factor gain vs. frequency offset, the frequency offset yielding the maximum Q-factor gain appears unchanged with α.

3.4. MRR design trade-offs

As shown in Fig. 7, the maximum Q-factor gain occurs at an offset that varies with κ, that is, a given frequency response $H(f)$ will lead to a different optimal offset. The best achievable performance for certain MRR designs occurs at small positive frequency offset, which means that the OFDM signal and carrier fall on the edge of the MRR response. By changing the scaling factor, we can keep the roll-off of a given choice of κ, but adjust the impact at a particular frequency. Working only with adjusting κ would require us to change the roll-off and therefore induce undesired affects at other frequencies.

For instance, if we tried to use a smaller κ, we would necessarily see a smaller extinction ratio, smaller full wave half maximum (FWHM) bandwidth and sharper roll-off, which would provide carrier suppression without much undesired filtering on the signal band. However, due to the small FWHM, the range in which we could suppress the carrier is also smaller. More precise wavelength control is also required for smaller κ MRRs. When trying larger κ, the roll-off is shallower, and we will suffer more undesired signal filtering, in order to achieve more carrier suppression. The tolerance to frequency drift will improve. Though not shown in the simulation, there is a limit to moving to smaller coupling ratio. A minimum extinction ratio is needed to achieve sufficient carrier suppression.

4. Experimental Results and discussion

Our first proof-of-concept experiment using silicon photonics cascaded microring resonators for SSBI cancellation was presented at MWP 2017 [12]. We present in this paper improved results using a notch shaped response in a single MRR. We first characterize the fabricated MRR. Then the subsystem, Y branch and MRR, is demonstrated experimentally.

4.1. Design and characterization of MRR

The new MRR consists of two straight waveguides and a single ring between them. The ring radius is 44.8 μm for a resonance peak near 1550 nm and free spectral range around 2 nm. The width and height of the waveguide are 500 nm and 220 nm respectively. The gap between the ring and straight waveguides is 200 nm on both sides. The coupling length of the directional coupler is 8 μm. The SiP chip is fabricated using a 220-nm silicon-on-insulator (SOI) process through the CMC Microsystem SiP MWP service. The lithography of the fabricated chip is at 193 nm.

We use a 25° fiber array to couple light into the chip to characterize our design. The coupling loss is around 15 dB. We sweep the laser frequency, and measure the power output to estimate the frequency response. After compensating for coupling loss, we fit the frequency response curve to simulated ones based on our design parameters. The simulated response of the two bus MRR is found using the transfer matrix method [15]. The ring radius and coupling length are set to design parameters, while the coupling coefficient κ is fitted, as described in the following. The coupling loss is assumed to be 3 dB/cm.

Due to fabrication errors, the central frequency and the response shape may vary from chip to chip. The blue curve with circle markers in Fig. 8 represents the measured response of the MRR used in experiments reported in the next section. We neglect the coupling loss in our simulations. We shift the measured central frequency to match the design target, i.e., the simulated central frequency. For $\kappa = 0.45$, we obtain the red curve (no markers) in Fig. 8. When testing five fabricated chips, the estimated coupling coefficient κ varied from 0.36 to 0.46. The extinction ratio is larger than 30 dB, and the full width half maximum (FWHM) bandwidth is around 18 GHz for the MRR used in the experiment reported in the next section.

For comparison, the third-order MRR used in [12] had a radius of 10 nm for each of its three

National Science and Engineering Research Council of Canada (NSERC) Funding: CRDPJ 499664

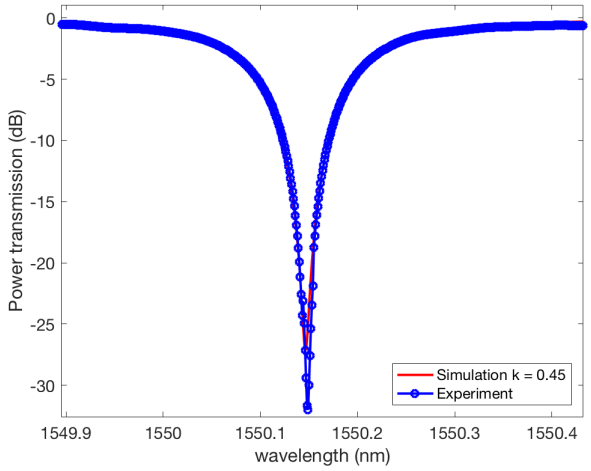

Fig. 8: Characterization of new MRR

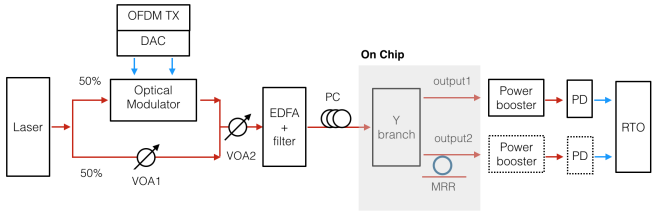

Fig. 9: Experimental Setup; as identical photodetectors were not available, a single photodetector is time multiplexed

component rings. The asymmetric coupler gap was 150 nm, while the gap between the rings are 180 nm. The coupling length of the directional coupler was 6 μm. Three resonance peaks were observed in every period. Two resonance peaks were used to as carrier suppression filters in that experiment. One had 17 dB extinction ratio and FWHM bandwidth is around 43.5 GHz. The other had an extinction ratio around 12 dB and FWHM around 25 GHz.

4.2. Experimental setup

Fig. 9 shows the experimental setup. A single-side-band OFDM signal, with 16 GBaud bandwidth, 256 subcarriers, and without guard band, is generated offline with MATLAB. The electrical QPSK signal is generated by a 64-GS/s digital-to-analog converter (DAC) with 15 GHz bandwidth and 8 bit resolution. The signal drives an SHF IQ modulator whose input is a laser with tunable wavelength and 100 kHz linewidth. The wavelength is tuned to achieve the desired frequency offset. We use two polarization-maintaining couplers and two variable attenuators (VOA) to adjust CSPR, as illustrated, having split the laser output. The IQ modulator is biased at the null point to generate a SSB carrier-suppressed OFDM signal. The total optical power is constant when adjusting CSPR.

The SSB-OFDM signal is coupled into the fabricated chip via grating couplers. Amplification stages are used at input and output to overcome coupling losses in the unpackaged chip. The EDFAs (erbium doped fiber amplifiers) are followed by a tunable optical band pass filter (OBPF) with 0.4 nm pass-band to remove amplified spontaneous emission before PD.

On-chip, we split the optical signal into two paths via a Y branch. The signal in one path is

National Science and Engineering Research Council of Canada (NSERC) Funding: CRDPJ 499664

transmitted unchanged, and then directly detected with an off-chip photodetector (PD). In the second branch, carrier suppression is realized by a two-bus MRR with a single deep notch. As the SiP components are sensitive to polarization, a polarization controller (PC) is used before the light is coupled into chip. The electrical signal after PD is captured by a real-time oscilloscope (RTO) with an 80 GS/s sampling rate, and then processed off-line with MATLAB. We reduce the sampling rate to two samples per symbol to mimic a realistic system. All processing is done at two samples per symbol.

Due to the lack of identical PDs, a single PD is time-multiplexed to convert the two chip outputs to the electrical domain in a round robin fashion. This leads to sub-optimal performance as the noise when using time-multiplexing is uncorrelated, while noise detected simultaneously on two identical PDs would cancel out. Therefore our results are somewhat pessimistic vis-à-vis the simulated identical PDs illustrated in Fig. 4.

4.3. SSBI cancellation

To visualize the efficiency of the SSBI cancellation procedure, we calculated the power spectral density of the signals in each branch, the through path and the carrier-suppressed path. For frequency offset of 12 GHz and CSPR of 0 dB, Fig. 10a shows the signal corrupted by SSBI noise (blue spectrum) and the estimated SSBI (yellow spectrum). Both spectra exhibit a triangular shape, as expected. The estimated SSBI has a lower intensity because the total power is diminished by filtering the carrier.

Fig. 10b recreates the signal corrupted by SSBI noise (blue spectrum), and superimposes the signal after SSBI cancellation (green spectrum). We trace two lines on each spectra to approximate the hypotenuse of the triangular spectra. Ideally we would have a flat, zero-angle spectrum. We can see that post-cancellation the spectra is flatter vis-à-vis the SSBI corrupted spectrum, with considerably reduced angle. The difference between the two spectra is an indication of the extent of SSBI reduction, the source of performance improvement.

As the residual SSBI varies across subcarriers, we expect performance per subcarrier to also vary. We transmit frames of 10^5 symbols, and estimate Q-factor using the method described in (1) and (2). For frequency offset of 12 GHz and CSPR of 0 dB, i.e., the spectra in Fig. 10, we calculate Q-factor per subcarrier and report it in Fig. 11. Without SSBI cancellation, we see the classic exponential Q-factor increases at higher-index subcarriers where the triangular SSBI spectrum has fallen to zero. The Q-factor is 4 dB for lowest-index subcarriers and increases to 14 dB.

After SSBI cancellation, all subcarriers have similar performance, as shown by the black curve in Fig. 11. While quite uniform, the higher-index subcarriers do see some degradation, though still improved performance compared to the case without SSBI cancellation. The suppression filter is most effective around the carrier frequency, i.e., in the region of lower-index subcarriers. Note that the optimal α factor (as defined in section III.C) is one. Due to the presence of an EDFA at the chip output, there is a power equalizing effect. A system with on-chip photodetection might see a different optimal α.

4.4. SSBI cancellation performance

We sweep the carrier wavelength to study the performance of SSBI cancellation at different frequency offsets. We also examine three levels of CSPR (0 dB, 3 dB and 5 dB) to assess SSBI cancellation performance for different SSBI strength.

Fig. 12 shows the experimental results for average (over subcarriers) Q-factor gain in dB versus frequency offset. For each point, we sweep α and report gain for the optimal α for that data point. We see the same behavior identified in simulations in Fig. 7. Negative frequency offsets see little gain. Centering the notch on the carrier, zero frequency offset, is not the best strategy. As predicted in the discussion of section III.A, a positive frequency offset provides the best mitigation of non-ideal filtering.

The three curves plotted in Fig. 12 are for various CSPR values, all yielding similar Q-factor gain.

National Science and Engineering Research Council of Canada (NSERC) Funding: CRDPJ 499664

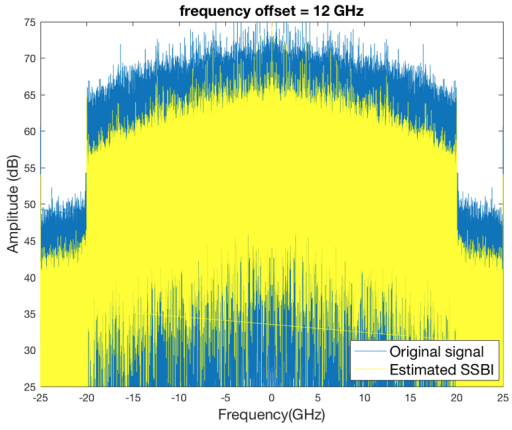

(a)

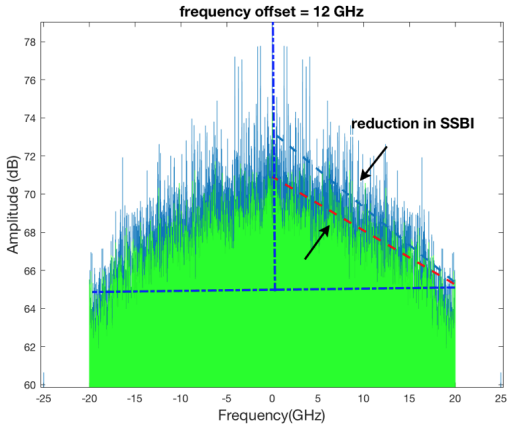

(b)

Fig. 10: Electrical spectrum of a) signal plus SSBI noise (blue/dark) and isolated SSBI (yellow/light colored), and b) signal plus SSBI noise (blue/dark) and signal with suppressed SSBI (green/light colored)

The gain is calculated with respect to Q-factor without SSBI cancellation: 4.74 dB for $CSPR = 0$ dB, 6.12 dB for $CSPR = 3$ dB, and 7.01 dB for $CSPR = 5$ dB. The simulation results in section III predict the frequency offset to achieve best cancellation performance shifts as the CSPR changes. Larger CSPR leads to better performance after cancellation than small CSPR values because a signal with larger carrier suffers less from SSBI. Thus the lower CSPR signal experiences higher Q-factor improvement.

For comparison, we recreate in Fig. 12 in square markers the previously reported [12] Q-factor improvement. That demonstration used a cascaded third-order MRR with a broadened frequency response, with smaller extinction ratio and larger FWHM bandwidth. Clearly the extinction ratio and roll-over has a strong impact on SSBI cancellation.

For all three CSPRs from 8-18 GHz offsets we see a uniform, high level of Q-factor gain. As MRRs are subject to temperature-induced frequency drift, this provides for more robust performance. Good levels of performance are obtained for all CSPR levels for a range of 12 GHz. The Q-factor after SSBI cancellation varies from 14.7 dB to 16.2 dB for offsets in between 8 GHz and 20 GHz, over the range of CSPRs.

National Science and Engineering Research Council of Canada (NSERC) Funding: CRDPJ 499664

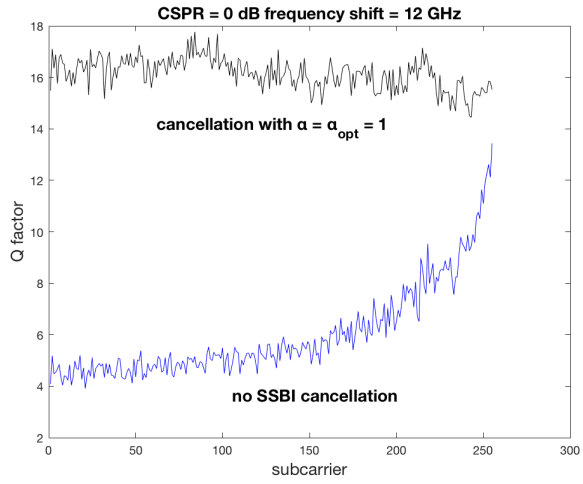

Fig. 11: Q-factor per subcarrier

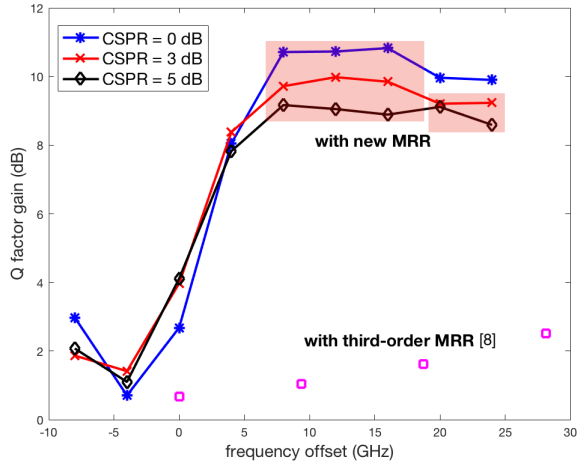

Fig. 12: Q-factor improvement [16] in dB due to SSBI cancellation vs. frequency offset for the three values of CSPR. Proof-of-concept demonstration [12] results in square markers are included for comparison.

5. Discussion

The experimental results shown in Fig. 11 and Fig. 12 confirm simulation predictions, and exhibit good performance after SSBI cancellation. Without SSBI cancellation, the Q-factor for all three CSPRs is below 8.5 dB. The 7% forward error correction (FEC) threshold of 3.8×10^{-3} is not achievable at that Q-factor, even for QPSK modulation. We would need to use significant guard band to avoid SSBI at these CSPR levels.

After cancellation, we can see significant Q-factor gain. As shown in Fig. 12, even with no guard band, we have a margin of 7.5 dB above the FEC threshold for QPSK over a large frequency offset range. The shaded part in Fig. 12 are points with Q-factor larger than 15.19 dB, where 16 QAM is possible considering the 7% FEC. With zero guard band and low CSPR, the optical suppression could achieve 64 Gbits/s over a 16 GHz bandwidth.The uniform performance of different subcarriers after our optical SSBI cancellation indicates that the SSBI is well cancelled.

National Science and Engineering Research Council of Canada (NSERC) Funding: CRDPJ 499664

Our performance should be compared to that of solutions offered by other researchers [17]–[21]. Traditional approaches include a strong carrier or a guard band to avoid SSBI. More recent DSP solutions include iterative cancellation and KK. To compare our solutions with these alternatives, we fix target data rate and OSNR and assume ideal probabilistic shaping and use theoretical calculations as in [18]–[21]. For a single polarization, single side band, direct detection system, from Shannon's formula the required bandwidth B for the analog to digital converter (ADC) is related to the data rate R by

$$R = \eta B \log_2 \left(\frac{OSNR}{1 + CSPR} \frac{B_{ref}}{B} \right) \tag{3}$$

where η is the spectral efficiency and B_{ref} is the reference bandwidth. We fix all other values and solve for B. We target a bit rate of $R = 200$ Gbits/s, assume a received OSNR of 30 dB, η of 0.5 for a guard band approach and 1 for other schemes, and $B_{ref} = 12.5$ GHz. In some architectures, a 3 dB penalty is imposed on the received OSNR.

For all SSBI suppression or mitigation methods, there will always be residual SSBI. To compare these techniques fairly, we assume the SSBI problem is completely suppressed with sufficient CSPR (that varies by suppression techniques). Table 1 shows the CSPR requirements (found experimentally in cited references) and ADC bandwidth requirements B calculated from (3).

Strategy against SSBI	Minimum CSPR (dB)	Number of PDs	Number of ADCs	Minimum ADC bandwidth (GHz)
Strong carrier [18]	15	1	1	78GHz
Guard band [19]	0	1	1	50.2GHz
Iterative SSBI cancellation [17]	9	1	1	38.3GHz
Kramer-Kronig receiver [20]	6	1	1	31.6GHz
Enhanced KK receiver [21]	3	2	2	33.4GHz
Hardware SSBI cancellation	0	2	1	29.7GHz

Table 1 : Comparison of CSPR and ADC requirements for different DD-SSB schemes with 30 dB received OSNR and 200 Gbits/s net data rate

When relying solely on a strong carrier power to make SSBI negligible, the required CSPR is 15 dB [18]. As a result, we need 78 GHz optical spectrum to achieve 200 Gbits/s, an ADC to cover the spectrum, and one PD. If we use a large guard band to avoid the SSBI, the spectral efficiency is halved, but the CSPR can be as low as 0 dB [19]. Invoking the formula, the ADC bandwidth requirement is 50.2 GHz to cover the guard band of 25.1 GHz. DSP methods including iterative SSBI cancellation and KK detection could reduce the CSPR to 9 dB and 6 dB respectively [17], [20], [21], leading to reduced ADC bandwidth requirements of 38.3 GHz and 31.6 GHz, respectively. With an enhanced KK receiver, smaller CSPR is required compared to traditional KK, however the received signal is split at reception, invoking a 3 dB OSNR penalty. The net effect is to increase the bandwidth requirement to 33.4 GHz. For our optical cancellation solution, as verified with our experiment, the CSPR could be reduced to 0 dB. Again, a 3 dB OSNR penalty is included given the y-branch splitting. The calculated ADC bandwidth requirement for optical SSBI cancellation is 29.7 GHz.

PONs are severely constrained in cost. For instance, single feeder PONs allow the uplink to be borne by the carrier distributed on the downlink. Low required CSPR means the limited carrier power can provide better performance on both the downlink and uplink. Components must also

National Science and Engineering Research Council of Canada (NSERC) Funding: CRDPJ 499664

be cost and power efficient in a PON. Higher bandwidth ADCs will significantly increase the deployment cost. Our solution provides the best solution vis-à-vis low CSPR, bandwidth efficiency and required ADC bandwidth.

Even while incurring a 3 dB loss in OSNR at the receiver front end in our solution, the lower CSPR requirement results in performance improvement. Among all direct detected SSB schemes, optical cancellation has the potential to realize the lowest required CSPR, as well as avoiding a large guard band. The only drawback is the use of two PDs to achieve balanced detection. The SiP solution and integrated PD means this additional complexity should only incur modest cost. Balanced detection offers the additional advantage of suppressing common mode noise.

Due to the polarization sensitivity of SiP components, we used polarization control in our demonstrations. In future designs, on-chip polarization splitter rotators would be included to achieve polarization diversity and obviate polarization control. For temperature stability, an additional on-chip PD and slow electronic feedback would be needed. Our MRR design provides a level of robustness against temperature induced frequency drifting, thus the feedback loop requirements would not be demanding.

6. Conclusion

We have fabricated and experimentally examined a SiP SSBI cancellation subsystem for DD-OFDM. System simulations confirmed the effectiveness of SiP SSBI cancellation and predicts the influence of frequency offset on SSBI cancellation. Experiments with the fabricated chip validates simulation results. We demonstrate significant Q-factor gain. The Q-factor can be increased to 15.57 dB, 16.09 dB and 16.19 dB, respectively, for CSPR = 0 dB, 3 dB, 5 dB. The spectral efficiency is high, as no guard band is used. Lower CSPR is required compared to both standard and enhanced KK, and no extensive DSP is needed as compared to the enhanced KK method. The SIP system offers low complexity and cost. Our subsystem is proved to be robust across a wide range of frequency offset via experiment.

7. Acknowledgement

We acknowledge CMC Microsystems for enabling the SiP fabrication.

References

[1] J. Yu, M.-F. Huang, D. Qian, L. Chen, and G.-K. Chang, “Centralized lightwave wdm-pon employing 16-qam intensity modulated ofdm downstream and ook modulated upstream signals,” IEEE Photonics Technology Letters, vol. 20, no. 18, pp. 1545–1547, 2008.

[2] S. Randel, D. Pilori, S. Chandrasekhar, G. Raybon, and P. Winzer, “100-gb/s discrete-multitone transmission over 80-km ssmf using single-sideband modulation with novel interference-cancellation scheme,” in Optical Communication (ECOC), 2015 European Conference on. IEEE, 2015, pp. 1–3.

[3] Z. Li, M. S. Erkilinc, L. Galdino, K. Shi, B. C. Thomsen, P. Bayvel, and R. I. Killey, “Comparison of digital signal-signal beat interference compensation techniques in direct-detection subcarrier modulation systems,” Optics express, vol. 24, no. 25, pp. 29 176–29 189, 2016.

[4] Z. Li, M. S. Erkilinc, R. Maher, L. Galdino, K. Shi, B. C. Thomsen, P. Bayvel, and R. I. Killey, “Two-stage linearization filter for direct-detection subcarrier modulation,” IEEE Photonics Technol. Lett., vol. 28, no. 24, pp. 2838–2841, 2016.

[5] Z. Li, M. S. Erkılınç, S. Pachnicke, H. Griesser, R. Bouziane, B. C. Thomsen, P. Bayvel, and R. I. Killey, “Signal-signal beat interference cancellation in spectrally-efficient wdm direct-detection nyquist-pulse-shaped 16-qam subcarrier modulation,” Optics Express, vol. 23, no. 18, pp. 23 694–23 709, 2015.

[6] Z. Li, M. S. Erkılınç, K. Shi, E. Sillekens, L. Galdino, B. C. Thomsen, P. Bayvel, and R. I. Killey, “Ssbi mitigation and the kramers–kronig scheme in single-sideband direct-detection transmission with receiver-based electronic dispersion compensation,” Journal of Lightwave Technology, vol. 35, no. 10, pp. 1887–1893, 2017.

[7] S. C. C. Mecozzi, Antonelli and Winzer, “The kramers-kronig receiver,” in Optical Fiber Communication Conference. Optical Society of America, 2018, pp. Tu2D–1.

[8] Z. Li, M. Erkilinc, K. Shi, E. Sillekens, L. Galdino, B. Thomsen, P. Bayvel, and R. Killey, “Joint optimisation of resampling rate and carrier-to-signal power ratio in direct-detection kramers-kronig receivers,” in Proc. ECOC, 2017.

[9] L. Blech, Y. Eldar, C. Antonelli, A. Mecozzi, and M. Shtaif, “The enhanced kramers kronig receiver,” in Optical Fiber Communication Conference. Optical Society of America, 2018, pp. Tu2D–7.

National Science and Engineering Research Council of Canada (NSERC) Funding: CRDPJ 499664

[10] W.-R. Peng, I. Morita, and H. Tanaka, "Enabling high capacity direct-detection optical ofdm transmissions using beat interference cancellation receiver," in Optical Communication (ECOC), 2010 36th European Conference and Exhibition on. IEEE, 2010, pp. 1–3.
[11] S. A. Nezamalhosseini, L. R. Chen, Q. Zhuge, M. Malekiha, F. Marvasti, and D. V. Plant, "Theoretical and experimental investigation of direct detection optical ofdm transmission using beat interference cancellation receiver," Optics express, vol. 21, no. 13, pp. 15 237–15 246, 2013.
[12] M. Lyu, X. Guan, and L. A. Rusch, "Experimental examination of ssbi suppression using sip microring resonators," in Microwave Photonics (MWP), 2017 IEEE International Topical Meeting on. IEEE, 2017, p. accepted to appear.
[13] L. Chrostowski and M. Hochberg, Silicon photonics design: from devices to systems. Cambridge University Press, 2015.
[14] R. A. Shafik, M. S. Rahman, and A. R. Islam, "On the extended relationships among evm, ber and snr as performance metrics," in Electrical and Computer Engineering, 2006. ICECE'06. International Conference on. IEEE, 2006, pp. 408–411.
[15] J. K. Poon, J. Scheuer, S. Mookherjea, G. T. Paloczi, Y. Huang, and A. Yariv, "Matrix analysis of microring coupled-resonator optical waveguides," Optics express, vol. 12, no. 1, pp. 90–103, 2004.
[16] M. Lyu, W. Shi, and L. A. Rusch, "Sip alternative to enhanced kk for ofdm," in 2018 European Conference on Optical Communication (ECOC). IEEE, 2018, pp. 1–3.
[17] X. Chen, S. Chandrasekhar, and P. Winzer, "Self-coherent systems for short reach transmission," in 2018 European Conference on Optical Communication (ECOC). IEEE, 2018, pp. 1–3.
[18] D. Hewitt, "Orthogonal frequency division multiplexing using baseband optical single sideband for simpler adaptive dispersion compensation," in Optical Fiber Communication Conference. Optical Society of America, 2007, p. OME7.
[19] A. J. Lowery, "Improving sensitivity and spectral efficiency in direct-detection optical ofdm systems," in Optical Fiber communication/National Fiber Optic Engineers Conference, 2008. OFC/NFOEC 2008. Conference on. IEEE, 2008, pp. 1–3.
[20] W.-R. Peng, X. Wu, V. R. Arbab, B. Shamee, L. C. Christen, J.-Y. Yang, K.-M. Feng, A. E. Willner, and S. Chi, "Experimental demonstration of a coherently modulated and directly detected optical ofdm system using an rf-tone insertion," in Optical Fiber communication/National Fiber Optic Engineers Conference, 2008. OFC/NFOEC 2008. Conference on. IEEE, 2008, pp. 1–3.
[21] W.-R. Peng, X. Wu, K.-M. Feng, V. R. Arbab, B. Shamee, J.-Y. Yang, L. C. Christen, A. E. Willner, and S. Chi, "Spectrally efficient direct-detected ofdm transmission employing an iterative estimation and cancellation technique," Optics express, vol. 17, no. 11, pp. 9099–9111, 2009.

National Science and Engineering Research Council of Canada (NSERC) Funding: CRDPJ 499664